Computers in Biology and Medicine 107 (2019) 73–85

Contents lists available at ScienceDirect

Computers in Biology and Medicine

journal homepage: www.elsevier.com/locate/compbiomed

3D segmentation of exterior wall surface of abdominal aortic aneurysm from CT images using variable neighborhood search

Thanongchai Siriapisith[a,b], Worapan Kusakunniran[a,*], Peter Haddawy[a,c]

[a] Faculty of Information and Communication Technology, Mahidol University, Nakhonpathom, Thailand
[b] Faculty of Medicine Siriraj Hospital, Mahidol University, Bangkok, Thailand
[c] Bremen Spatial Cognition Center, University of Bremen, Bremen, Germany

ARTICLE INFO

Keywords:
Abdominal aortic aneurysm
Computed tomography
3D reconstruction
3D segmentation
Iterative
Graph cut
Probability density function
Variable neighborhood search
3D model

ABSTRACT

A 3D model of abdominal aortic aneurysm (AAA) can provide useful anatomical information for clinical management and simulation. Thin-slice contiguous computed tomographic (CT) angiography is the best source of medical images for construction of 3D models, which requires segmentation of AAA in the images. Existing methods for segmentation of AAA rely on either manual process or 2D segmentation in each 2D CT slide. However, a traditional manual segmentation is a time consuming process which is not practical for routine use. The construction of a 3D model from 2D segmentation of each CT slice is not a fully satisfactory solution due to rough contours that can occur because of lack of constraints among segmented slices, as well as missed segmentation slices. To overcome such challenges, this paper proposes the 3D segmentation of AAA using the concept of variable neighborhood search by iteratively alternating between two different segmentation techniques in the two different 3D search spaces of voxel intensity and voxel gradient. The segmentation output of each method is used as the initial contour to the other method in each iteration. By alternating between search spaces, the technique can escape local minima that naturally occur in each search space. Also, the 3D search spaces provide more constraints across CT slices, when compared with the 2D search spaces in individual CT slices. The proposed method is evaluated with 10 easy and 10 difficult cases of AAA. The results show that the proposed 3D segmentation technique achieves the outstanding segmentation accuracy with an average dice similarity value (DSC) of 91.88%, when compared to the other methods using the same dataset, which are the 2D proposed method, classical graph cut, distance regularized level set evolution, and registration based geometric active contour with the DSCs of 87.57 ± 4.52%, 72.47 ± 8.11%, 58.50 ± 8.86% and 76.21 ± 10.49%, respectively.

1. Introduction

Abdominal aortic aneurysm (AAA) is an abnormal dilatation of the abdominal aorta, which can cause rupture leading to death. Epidemiological studies in the United States have revealed that AAA is a disease of increasing incidence and mortality, with major risk factors being hypertension, high cholesterol and smoking [1,2]. More than 10,000 people die from rupture each year [3,4]. Aortic rupture typically occurs in the abdominal region [4] and is commonly associated with large size or complex shape. Because of this, 3D surface models are more reliable than maximum cross sectional diameter [5] in predicting the likelihood of AAA rupture on a patient specific-basis. 3D models of AAA can provide useful information for clinical management and simulation, such as pre-operative planning for endovascular stent grafting, shear wall stress evaluation for predicting risk of rupture and arterial flow simulation.

To obtain a 3D model, segmentation of the AAA is required. The anatomical structure of an AAA is composed of inner and outer walls, and thrombus between them. The segmentation of the outer wall of AAA is particularly challenging because the outer wall is typically asymmetric around the inner wall and has complex anatomy. For complex shaped AAA, 2D segmentation is not suitable because it is typically inaccurate at steep contour points, exactly those areas where high precision is desired. In addition, its image intensity is very similar to neighborhood tissues, which leads to low gradient differences at the boundary of the outer wall and other neighboring structures. The segmentation of difficult cases is yet an open problem. Thus, we focus on the segmentation of outer wall of AAA in both easy and difficult cases.

In previous work [6] we introduced the use of the combination of intensity-based and gradient-based segmentation to solve the problem

* Corresponding author.
E-mail address: worapan.kun@mahidol.edu (W. Kusakunniran).

https://doi.org/10.1016/j.compbiomed.2019.01.027
Received 23 November 2018; Received in revised form 15 January 2019; Accepted 30 January 2019

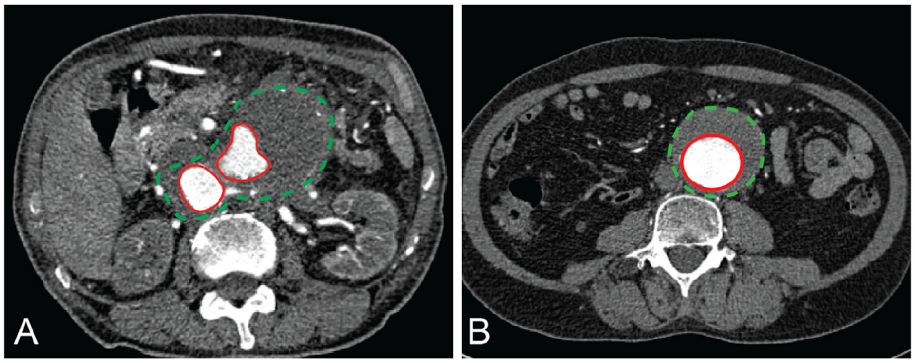

Fig. 1. Source CT images of abdominal aortic aneurysm in various shapes. The aneurysm shape is not always round. Most of the cases are oval shape and eccentric thrombus. (A) An example of oval shape with eccentric thrombus of aneurysm. (B) An example of round shape with eccentric thrombus of aneurysm. Dotted green lines represent the outer walls and solid red lines represent the inner walls.

of outer wall segmentation of AAA in 2D grayscale CT images. The AAA segmentation was independently performed in each CT slice and then assembled into a 3D model. This technique successfully addresses the problem of similarity of outer wall pixel intensity with that of surrounding tissue. But the 2D segmentation has several limitations. The most obvious limitation occurs with severe tortuosity of aneurysm, which shows two inner lumens and bizarre outer wall in CT slice (as shown in Fig. 1). While a 3D model can be constructed from independently segmented 2D CT slices, this typically results in a 3D model with a very noisy surface. For example, 2D segmentation can overestimate and underestimate in some slices, causing stepping in the constructed 3D model. The contour smoothness can be improved by applying interpolation but the resulting 3D model does not fit well with the real outer wall. In this paper, we generalize our previous 2D algorithm to apply to 3D segmentation in the full 3D search space.

1.1. Main contributions

This paper focuses on 3D segmentation of the outer wall of AAA on 3D CT datasets. We propose a novel 3D segmentation based on intensity and gradient search spaces. These two search spaces are combined using variable neighborhood search (VNS) [7–9] and graph-cut structures, where the local minima that commonly occur in each search space can be escaped from by switching to the other search space. Our method is a fully automatic segmentation approach in the 3D environment, which can successfully segment complex shaped aneurysms on which 2D techniques fail. To the best of our knowledge, this paper is the first to perform fully automatic 3D segmentation of AAA using 3D datasets reconstructed from contiguous CT slices. The segmentation performance was evaluated against ground-truth obtained from manual segmentation by human experts. The proposed method is shown to have state-of-the-art performance.

1.2. Related work

Various imaging modalities have been used for visualization of aortic aneurysm such as ultrasonography, computed tomography (CT), and magnetic resonance imaging (MRI). Segmentation of aortic aneurysm from CT is much more difficult than from MRI, because the CT is density-based imaging which is not as distinct as the tissue-based MR images. It is well known that the tissue distinguishability is typically clearer on MR images than CT images. Nonetheless, CTA is currently the most widely used imaging modality in patients with suspected aortic disease, particularly in emergency situations. Several studies have addressed outer wall segmentation of abdominal aorta on contrast enhanced CT images [10–16]. Basic methods of AAA segmentation operated on 2D slices. Shum et al. [10] proposed a semi-automated algorithm in the 2D space to define the wall thickness in patients with AAA based on intensity histograms. It generated an array of isolines of pixel intensity on enhanced abdominal CT images. Additional manual correction was still needed for the final outer wall segmentation. Shang et al. [11,12] also segmented the outer wall using a semi-automated method in 2D space by detecting isointensity contours in contrast enhanced CT images of abdominal aorta. Their algorithm detected large changes of intensity in small areas which were likely to be transition zones between the outer wall and surrounding tissue. de Bruijne et al. [13] proposed a semi-automatic process of outer wall segmentation in CTA by a 2D active shape model, derived from manually labeled training images. The manual delineation was performed in the first slice, and then an automatic process was applied to segment the subsequent slices based on the grayscale similarity. Manual correction was also necessary in the region where adjacent tissue was very similar to the outer wall. A machine learning technique for post-operative AAA segmentation was proposed by Lpez-Linares et al. [17]. This technique was based on a fully convolutional neural network (CNN) and holistically-nested edge detection. The aim of their method was to solve the problem of parameter tuning and user interaction. However, the CNN approach requires a large amount of training data for each organ.

Techniques for segmentation of AAA in 3D space have operated with manual initialization/interaction or with only partial 3D segmentation. Lee et al. [14] proposed a semi-automatic process for outer wall segmentation in CTA using 3D graph search based on triangular mesh at the surface of the candidate outer wall. Additional manual control points were required during the segmentation process. Olabarriaga et al. [15] proposed outer wall segmentation in CTA using a 3D discrete deformable model based on grayscale level information of the thrombus. Manual interaction was required for training the classifier and for upper and lower slices of targeted vessel segmentation. Zhuge et al. [16] proposed automated 3D level set based segmentation of outer wall of AAA in CTA. However, the segmentation was not a fully 3D method. For the region analyzer in the global region analysis, the surface initialization and the local feature analysis steps relied on only the 2D space.

Other studies have demonstrated that 3D segmentation in other domains (general color image and video processing) has potential to improve the segmentation result as compared with 2D segmentation [18,19]. Recently, 3D graph cut segmentations were also successfully performed in various medical datasets, such as esophagus [20], liver [21,22], lung [23,24] and kidney [25]. Grosgeorge et al. [20] proposed a graph-cut based method with prior shape model for esophagus segmentation. They combined 3D with 2D segmentation. The 3D segmentation usually overestimated the results. Additional 2D segmentation was used to correct the overestimation and improved the results. Eapen et al. [21] proposed liver segmentation by 3D graph-cut. Manual user-specified regions for sampling foreground and background were required for the initialization. Massoptier et al. [22] also proposed liver segmentation by 3D graph-cut with a different method of initialization. The region for foreground was defined in the range of mean ± standard deviation. Jungwon et al. [23,24] proposed lung nodule segmentation by 3D graph-cut with prior shape information for initialization. The prior shape information was derived from the active shape model. Yoruk et al. [25] proposed renal segmentation for MR

urography by 3D grabcut. The initialization was based on mean and standard deviation values of the kidneys. This paper is the first to provide an algorithm for fully automated 3D segmentation of the outer wall of AAA in a 3D CTA dataset. The main concept of the proposed segmentation method is the iterative combination of gradient and intensity based segmentation techniques. Both segmentation methods are implemented based on graph structures, which can be applied with any number of dimensions, including 3D.

2. Proposed method

2.1. Overview of the proposed segmentation algorithm

The objective of the proposed method is to segment the outer wall of AAA in both easy and difficult cases of grayscale CT images. In practice difficult cases are commonly found involving tortuous shape and abundant soft tissue structures contacting the outer wall. The segmentation of difficult cases is yet an open problem. The proposed method is fully automatic under the 3D environment, based on the graph-cut segmentation. We combine intensity and gradient-based segmentations in each iteration based on the concept of VNS. In order to segment the outer wall, an initial contour is required as a starting point of the segmentation. This can be derived from the inner lumen, a region of flowing blood, which is significantly enhanced on the post-contrast CT images. It can therefore be easily segmented by simple thresholding.

The initial contour is obtained by dilatation of the inner lumen in order to cover the entire outer wall of AAA. Starting from the initial contour, two different segmentations in the two 3D-searching spaces are iteratively performed. The first layer segmentation is based on the intensity-based segmentation technique, called graph cut with probability density function (GCPDF), constructed using the 3D graph. Because of the lack of color information to distinguish the foreground from the background, this technique is better suited to grayscale images than classical graph cut or GrabCut [26–28]. The second layer segmentation relies on the contour-based technique, called graph cut based active contour (GCBAC), which detects the boundary of an object depending on the gradient difference of the adjacent voxels [29]. The GCBAC is also constructed in the 3D graph structure. In each iteration, GCPDF is used to partition the image using pixel intensity and GCBAC is then used to find the closest boundary in the closed space from the initial contour using the pixel gradient. This combination enables the segmentation of the outer wall of AAA with high accuracy. Because both segmentations use the contour as the initialization, they can be interchanged. The algorithm terminates when the flow in graph is steady. The algorithm terminates when the flow in the graph no longer changes from one iteration to the next. Since we alternate between algorithms to escape local minima, the stopping criterion is that the flow in both GCPDF and GCBAC does not change, indicating that a minimum has been reached in both search spaces. The final result is the segmented outer wall of AAA as a 3D model. The proposed framework is shown in Fig. 2.

2.2. Preprocessing

In general, CT images are contiguous transverse 2D slices through the patients body that require preprocessing as the first step to merge the 2D CT images into one 3D dataset. From the 3D dataset, the next preprocessing step is to carry out segmentation of the inner lumen. The inner lumen R_L has high intensity value due to the enhancement of the post-contrast images. Thus, the aortic inner lumen R_L can be segmented by a simple thresholding operation $L_T(p)$: $P \rightarrow \{0,1\}$

$$L_T(p) = \begin{cases} 1, & \text{if } p \geq th_{lumen} \\ 0, & \text{otherwise} \end{cases} \quad (1)$$

where th_{lumen} is the optimum threshold value for the aortic inner lumen and p is the pixel value.

To distinguish the inner lumen R_L from other high intensity soft tissue, the circular Hough transform [30] is applied to the first slice followed by regional growing detection on the subsequence slices.

After the inner lumen segmentation, the initial contour of the outer wall is created by dilation of the segmented inner lumen. The initial dilation is performed in the 3D space. That is the dilation is performed in all x, y and z planes. The dilation factor is calculated based on the xy-plane diameter of the segmented inner lumen. The dilation factor is set to be 2 in most of the cases. For the cases of the large size of aneurysm, setting the dilation factor to be 3 can result in better performance. In addition, the dilation factor is only set once for each case, and then used for all slides in the case.

2.3. Graph cut as the optimization tool

The graph cut approach has been widely applied as the global optimization method to solve the problem of image segmentation [27,28,31–33]. The graph cut creates a binary partition of the image into foreground and background. Each node of the graph represents each pixel in the image, while the edge weight between any two adjacent nodes can be assigned based on features such as the gradient difference or the intensity similarity between the two pixels. Cutting the graph based on the max-flow/min-cut algorithm generates the segmentation. The graph cut problem is to binary partition the nodes in the graph into two disjoint sets S and T such that source node $s \in S$ and sink node $t \in T$ [34]. The min-cut algorithm is to find the cut C with the minimum cost in graph. Referring to the theorem of Ford and Fulkerson [35], the min-cut is equivalent to the max-flow from the source to sink nodes in any graph.

The graph structure can be easily extended from a 2D graph to a 3D or higher dimensional graph. In the 3D problem, the edge capacities in the 3D dataset can be represented with the 6-26-connectivity to neighboring voxels (Fig. 3). The 6-connectivities are edge connections to neighboring voxels in $x+$, $x-$, $y+$, $y-$, $z+$ and $z-$ directions and 26-connectivities are edge connections to neighboring voxels in x, y, z and orthogonal directions. The classical use of energy minimization is to solve the voxel-labeling problem. The input is a set of voxels P and a set of labels L. The cost function to be minimized is the summation of the weights of the edges that are cut. The cut partitions the nodes V in the graph G into two subsets, S and T such that $s \in S$ and $t \in T$, where s and t are special additional source and sink nodes, respectively. The partitioning can be represented by a labeling f mapping from the set of the nodes $V - \{s, t\}$ to $\{0, 1\}$, where $f(v) = 0$ means that $v \in S$ and $f(v) = 1$ means that $v \in T$. A standard form of the energy function [34] is as below.

$$E(f) = \sum_{p \in P} D_p(f_p) + \sum_{p,q \in N} V_{p,q}(f_p, f_q) \quad (2)$$

where $N \in P \times P \times P$ which is a 3D neighborhood space on voxels, $D_p(f_p)$ is a function measuring the cost of assigning the label f_p to the voxel p representing a region term, and $V_{p,q}(f_p, f_q)$ is a function measuring the cost of assigning the labels f_p, f_q to the adjacent voxels p, q which is used to impose spatial smoothness or a boundary term.

2.4. Graph cut with probability density function

The main objective of using GCPDF in this proposed segmentation method is to partition the image or volume dataset into two subsets based on voxel intensity. To accomplish this, an undirected weighted graph $G = (V, E)$ is constructed, which is composed of a set of nodes V and a set of undirected edges E. The nodes v in V are assigned to voxels $p \in P$. The classical graph cut is modified by adding a probability density function to the edges e in order to partition the voxels which have intensity significantly higher or lower than the mean value inside the initial contour and outside the inner lumen. The probability density

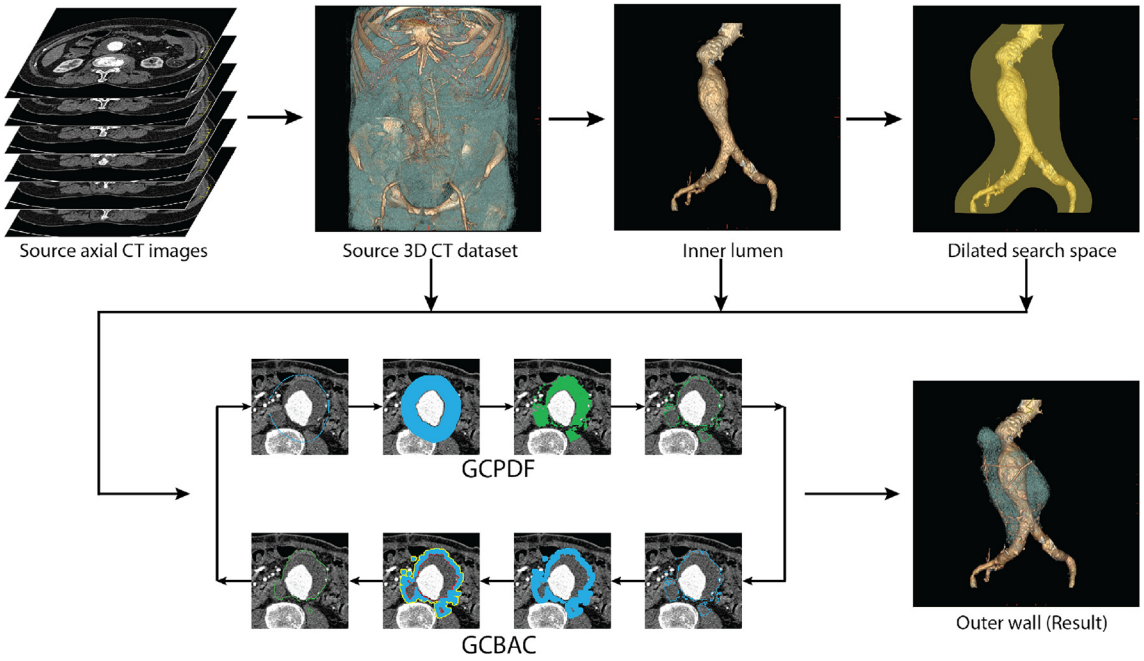

Fig. 2. Illustration of the proposed framework including two layers of iterative segmentation, composed of graph cut with probability density function (GCPDF) and graph cut based active contour (GCBAC). The outer part of the segmentation is the outer wall of the abdominal aortic aneurysm.

function is used to model the voxel intensity of possible foregrounds. The graph G is constructed with voxels in the region inside the initial contour (R_I), excluding the inner lumen. The edge weight to the source node $w(u, s)$ is assigned according to the probability of the pixel intensity of node u to be a source node using the probability density function, as below.

$$w(u, s) = \frac{1}{\sqrt{2\alpha\sigma^2\pi}} e^{-\frac{(x-\mu)^2}{2\alpha\sigma^2}} \tag{3}$$

where x is the voxel intensity, μ is the mean intensity, σ is the variance, α is a weighting factor of variance. The μ and σ are calculated from all voxels in the search space.

Correspondingly, $w(u, t)$ is the inverse normalized value of $w(u, s)$ with range from 0 to 100. The edge weight $w(u, v)$ is assigned by measuring voxel similarity between two adjacent voxels. The simple image gradient map using standard deviation in a small local region ($3 \times 3 \times 3$ voxels) is used to measure the voxel similarity, with the following equation.

$$w(u, v) = \frac{100}{\sqrt{E[x^2] - (E[x])^2}} \tag{4}$$

where $E[x]$ is the expected value of x.

Based on the 3D graph structure, each node has 6-connectivity to neighboring nodes and 2-connectivity to terminal nodes. The output region of segmentation $R_O = \{L_{GC}(p) = 1\}$ defines the region of thrombosis inside the aneurysm. The outer boundary of R_O is the output contour for the next iteration. Each node in the graph represents a voxel inside the contour, excluding the aortic lumen region (R_L). The source and sink nodes are added to graph G. The weighted edges from each node to the source, sink and adjacent voxel nodes are calculated. The air and bone regions are also directly removed voxel by voxel from the graph before processing the segmentation. The air or bone regions are defined by very low or high voxel intensity values, respectively. They could be detected by simple image thresholding. If a voxel is definitely bone or air, the corresponding node is removed from the graph. Then, the max-flow/min-cut algorithm is performed to partition the remaining nodes in the graph. The new label is updated to the regions

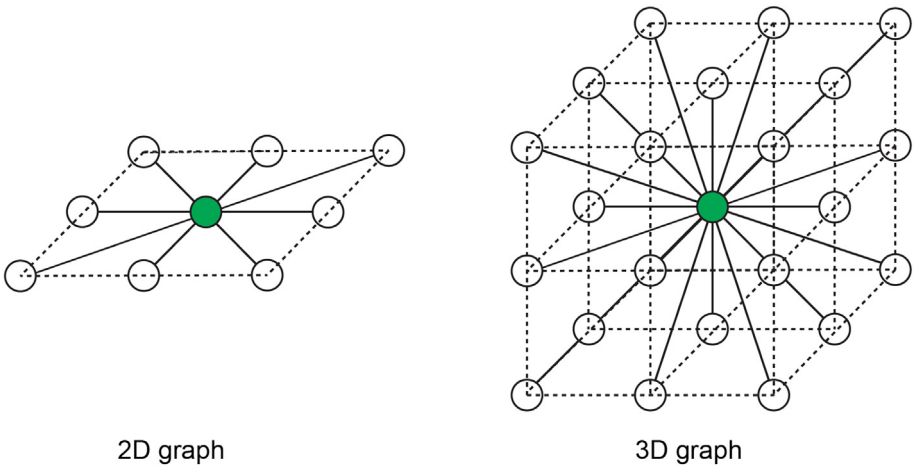

Fig. 3. Illustration of node connectivity in 2D and 3D graph. The 2D graph shows 6-connectivity from center to neighboring node. The 3D graph shows 26-connectivity from center to neighboring node in x, y, z and orthogonal directions.

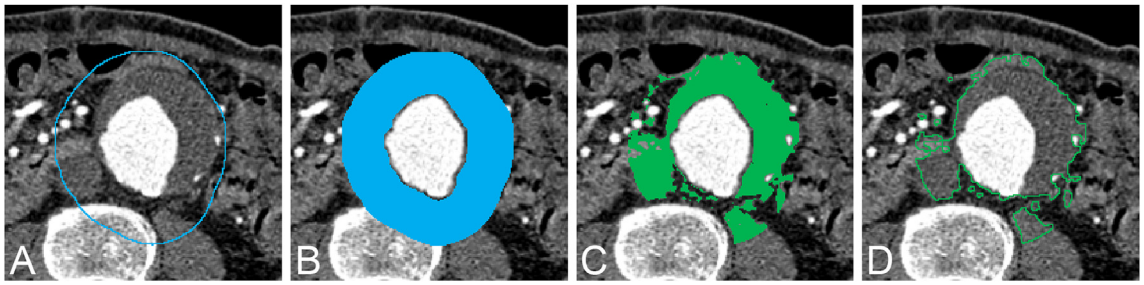

Fig. 4. An example of graph cut with probability density function. This illustration of segmentation was shown in transverse cut of the 3D dataset. (A) The initial contour for the segmentation. (B) The label region inside initial contour as search space. For the graph construction, each pixel in the region is represented by a node in the graph. (C) The output label region of segmentation using max-flow/min-cut algorithm. (D) The output contour of segmentation corresponds to the outer boundary of (C).

which are connected to the source node. To remove noise and fill holes in the output region, dilation is used with a structuring element of size $3 \times 3 \times 3$ voxels. The outer boundary of the output region is the resulting contour, as shown in Fig. 4.

2.5. Graph cut based active contour

In the second layer of the segmentation, graph cut based active contours (GCBAC) is applied. The GCBAC performs object segmentation based on the idea of deformation of active contours using the graph cut for energy minimization. Given an initial contour, it dilates to a belt-shaped contour neighborhood (CN) of a fixed width. The CN voxels overlapping with aortic inner lumen are eliminated from the CN. The GCBAC algorithm creates the new contour with the global minimum within the CN. An undirected weighted graph $G = (V, E)$ is constructed from each voxel in CN. Each pixel within the image is mapped to a node $u, v \in V$. The voxels that are located in the inner border (IB) and outer border (OB) of CN are defined as multiple source s and sink t in graph G, respectively. For this construction, the converted graph has a larger number of terminal nodes than the classical one that has an adverse impact on the time complexity of the minimum cut algorithm. For this reason, all of the nodes along IB are merged to a single source s_i, and all of the nodes along OB are merged to a single sink t_i. A simple operation called node identification is used to convert a graph of interest $G(V, E)$ to $G(V, E)$. The edge weight $w(u, v)$ between two adjacent voxels is assigned as the voxels similarity, as below.

$$w(u, v) = \varepsilon(g(u, v) + g(v, u))^{\gamma} \tag{5}$$

$$g\left(u, v\right) = exp\left(-grad_{u,v}\frac{u}{max_k(grad_{u,v}(k))}\right) \tag{6}$$

where $grad_{u,v}(k)$ is the magnitude of the voxel intensity gradient at the location k in the direction of $u \rightarrow v$. γ is the power magnitude of gradient, and ε is the weighted factor of the edge weight. The value of $grad_{u,v}(k)$ in the entire dataset is used to normalize the gradient magnitudes.

The edges in the graph represent neighborhood voxels. For the 3D model/structure, each node $v \in V$ in graph G, corresponding to a voxel p, which has edges connecting to the 26 neighboring nodes and corresponding to the 26 neighboring voxels of p. The output is the new contour along the minimum of graph G, as demonstrated in Fig. 5.

3. Experiments and results

The experiments were performed on an Intel Xeon E5-2697 v3 2.6 GHz CPU and 128 GB RAM64-bit running the Microsoft Windows 7 Operating System. The datasets were processed by the OpenCV software version 2.4.13 in Microsoft Visual Studio Express 2013. The manual ground-truth segmentation of outer wall of AAA in all axial slices was performed using the 3D slicer software version 4.7.0 by two cardiovascular radiologists with 15 and 11 years of experience, respectively.

3.1. CT imaging data

The datasets were acquired from 20 patients with AAA on whom contrast enhanced CTA was performed. The exclusion criteria were post open surgery, post endovascular aortic repair, impending rupture, rupture, intramural hematoma, dissection, mycotic aneurysm and poor contrast enhancement of abdominal aortic aneurysm. All CTA acquisition was performed with the 64-slice multi-detector row CT scanner (Somatom Definition; Siemens Medical Systems, Forchheim, Germany or Lightspeed CVT; GE Medical Systems, Milwaukee, Wisconsin, United States). All CTA acquisitions were performed using nonionic monomer iodinated contrast medium. The source axial CT images were reconstructed at 1 or 1.25 mm slice thickness from the level of renal to iliac in order to cover the entire AAA region. The total number of axial CT images for each case was 200 images for 1 mm thickness and 150 images for 1.25 mm thickness. The matrix resolution for each axial CT image was 512×512 pixels. The window width/level of CTA dataset was set in a range of 400–500/40–100 Hounsfield Units (HU) depending on different cases. The source CTA dataset was normalized from HU to 0–255. For the aortic inner lumen segmentation, the th_{lumen} for aortic inner lumen extraction was set at 180. There were two setting cases of th_{lumen} at 120 and 150.

The patients were categorized into two groups of ten patients each. The first group contained easy cases for the segmentation, while the second group contained difficult cases for the segmentation. The easy cases were defined as outer wall non-contiguous with adjacent soft tissue structures (bowel, muscle, other soft tissues), round or minimal oval shaped aneurysm (aneurysm aspect ratio ≤ 1.2) and thin thrombus (thrombus thickness ≤ 2.5 cm). This provides a clear boundary of the outer wall. The difficult cases were defined as outer wall contiguous with adjacent soft tissue structures, pronounced oval shaped aneurysm (aneurysm aspect ratio > 1.2) and thick thrombus (thrombus thickness > 2.5 cm). This is difficult partly because the outer wall is in contact with other structures with low gradient and intensity differences at the boundaries.

3.2. Parameter optimization for the segmentation

The initial contour of the outer wall segmentation was created by dilating the segmented inner lumen. To prevent over dilation, the initial dilation was performed in 2D. The dilation factor was 2 in 16 cases. For the remaining 4 cases, the dilation factor of 2 was not large enough to cover the outer wall, thus the factor was set to be 3. To prevent oversize dilation at upper and lower edges of the dataset (non-aneurysm portion), the dilation factor was fixed at 0.5. The upper and lower edges of the dataset were defined by 20% of the total number of slices for each edge. To eliminate the well-known structure of inferior vena cava

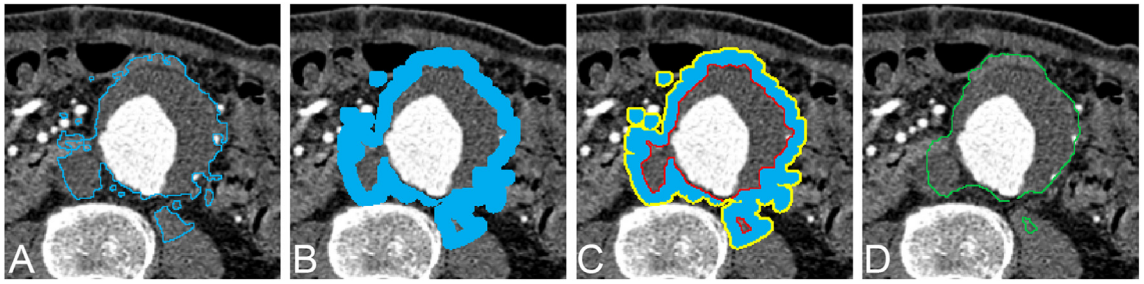

Fig. 5. An example of graph cut based active contour. This illustration of segmentation is shown in the transverse cut of the 3D dataset. (A) The input contour of the segmentation. (B) Dilate contour to contour neighborhood for the graph cut segmentation. (C) Label outer and inner boundaries of contour neighborhood to be source and sink nodes, respectively. (D) Output contour of the segmentation.

located on the right side of the aorta, the initial contour was shift to the left 10 or 20 voxels, depending on the size of aneurysm.

For the GCPDF, the weighted factor of variance α in Eq. (3) is 0.25, 0.5, 1. The parameter α represents the width of Gaussian distribution from $\mu - \sigma^2$ to $\mu + \sigma^2$. A larger α value means more variation of voxel intensity in the search space which represents the higher probability to include other structures in the segmentation. The thrombus inside the aneurysm usually has uniform voxel intensity and less variation. The optimal parameter α in this experiment was 0.5.

For the GCBAC, the parameter settings are β = 7, 9, 11, γ in Eq. (5) = 6, 18, 24 and ε in Eq. (5) = 0.2, 0.5, 1. The parameter β represents the voxel width in the CN search space. Larger β values result in wider area of the search space in GCBAC. According to the behavior of GCBAC, larger β values may get worse contour results that contact to the other strong image gradients and also increase the computation time. The optimal β value in this experiment was 7, 9 and 11. The parameter γ represents magnitude of the gradient between adjacent voxels. In the 2D GCBAC experiment by Xu et al. [29], the optimal value was 6. But in the 3D GCBAC, 6 is not strong enough because all image slices are constructed in one graph and each image slice will affect other slices. The optimal parameter γ in this experiment was 18, 24. The parameter ε defines the weighting factor of gradient difference strength between adjacent voxels. In the isotropic 3D graph, parameter ε is set to 1, whereas in the anisotropic 3D graph, the anisotropic weighted edge is modified in a range from 0 to 1. At the curvature or bifurcation of the aorta in some datasets, the resulting contour is directly in the oblique direction from aorta above the bifurcation to the iliac artery, which is the shortest path in the graph and not curved along the aortic bifurcation. For this reason, the orthogonal direction of weighted edge $w(u, v)$ (8 from the 26 edges connecting to neighboring nodes) is set up $x! = x$, $y! = y$ and $z! = z$, and the γ is 0.2. An example of the proposed segmentation in each iteration is shown in Fig. 6.

The performance of our proposed segmentation algorithm is compared with the performances of the following classical and recent advanced methods. These include the classical graph-cut (GC) which was commonly used in medical image segmentation [20–26], as well as the recently proposed distance regularized level set evolution (DRLSE) which showed good results on the outer wall segmentation of AAA [36]. The proposed method was also compared to the registration based geometric active contour (RGAC) [37,38] Chen et al. [37] segmented the outer wall of giant intracranial aneurysm using a geometric active contour (GAC) related method and reported the good result. Wang et al. [38] developed the method of the outer wall segmentation, called RGAC. Based on GAC and the manual delineation of the outer wall in the first slice, the GAC was applied to the subsequent slices, using the initial information from previous slice. Because of the limitation of DRLSE and RGAC on the 3D segmentation (i.e. it was designed for the 2D segmentation), these two methods are performed on 2D model/graph structure. Some of important parameters are listed as follows.

For the DRLSE, the coefficient of the distance regularization, weighted length, and the area terms are 1.5, 2.0 and 1.5, respectively. The algorithm was performed on each slice individually. The initial contour in each slice is generated from the dilation of the segmented inner lumen 2–4 times depending on the size of aneurysm.

For the RGAC, the GAC parameters in RGAC segmentation are α, β, γ, κ. They are set to be 0.8, 0.8, 0.8 and 6.0 respectively. The first slice was initialized by the manual delineation. The RGAC automatically detected contours in subsequent slices, based on the segmentation result from the previous slice. If the segmentation failed on a slice, the re-initialized by the manual delineation was needed on that slice.

3.3. Quantitative evaluation

The result evaluation was quantitatively evaluated by the comparison with the reference standard using the, true positive rate (TPR), dice similarity coefficient (DSC), Jaccard similarity coefficient (JSC) and false negative rate (FNR).

$$\%\text{True positive rate} = \frac{|R_A \cap R_R|}{(|R_R|)} \times 100 \tag{7}$$

$$\%\text{Dice similarity coefficient} = \frac{2|R_A \cap R_R|}{(|R_A| + |R_R|)} \times 100 \tag{8}$$

$$\%\text{Jaccard similarity coefficient} = \frac{|R_A \cap R_R|}{|R_A \cup R_R|} \times 100 \tag{9}$$

$$\%\text{Volume difference} = \frac{|R_A - R_R|}{\frac{1}{2}(R_A + R_R)} \times 100 \tag{10}$$

$$\%\text{False negative rate} = \frac{|R_R - R_A|}{(|R_R|)} \times 100 \tag{11}$$

where R_A is the region of segmentation result and R_R is the region of reference standard by manual segmentation.

3.4. Experimental results

Most recent studies have also used manual segmentation as the gold standard for evaluating the results of AAA segmentation algorithms [14–16,38]. In this experiment, the gold standard was produced by manual drawing of the aneurysm slice by slice by one experienced cardiovascular radiologist. The inter-observer agreement was obtained by manual drawing of the same 40 CT slices (2 slices for each case) by the two radiologists. The interobserver correlation was found to be 97.68 ± 0.82% which indicates excellent correlation. The total of 20 cases were manually drawn by only one radiologist, with the total number of slices being 3650 (150 slices for 7 cases and 200 slices for 13 cases). The iliac branches were also included in the segmentations.

The parameter optimizations of the proposed method are also performed. The α parameter in GCPDF is varied at 0.25, 0.5 and 1. Three parameters in the GCBAC part of the proposed method are voxel width in the CN, power magnitude of gradient and the anisotropic weighted

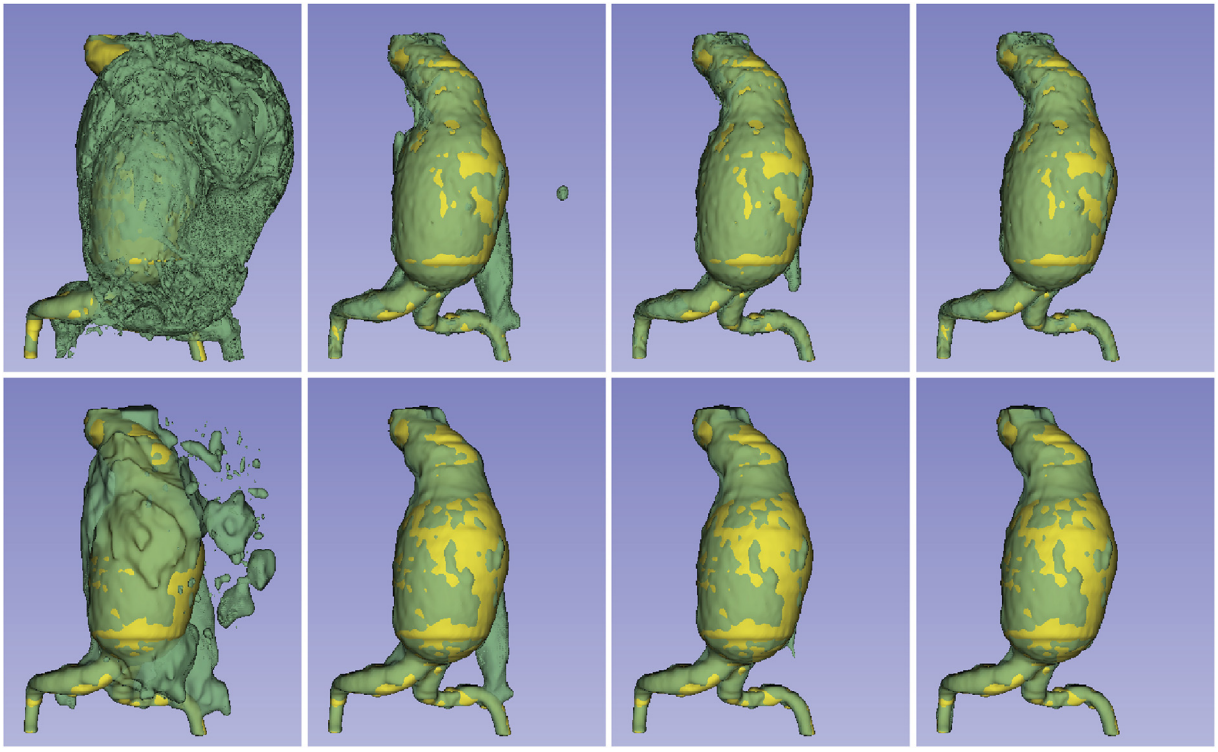

Fig. 6. Example 3D segmentation result in each iteration. The upper row is the result from the graph cut with probability density function and lower row is the result from the graph cut based active contour. From the left to right columns are 1st, 5th, 10th, and 15th iterations, respectively. The segmentation result (i.e. green color) is progressively converged and well matched to the ground-truth (i.e. yellow color).

Table 1
Quantitative evaluation of proposed segmentation result by comparison with reference standard (manual segmentation). The easy and difficult cases were performed with contour neighborhood voxel size = 7 and 11, respectively. The weighted factor variance (α) in graph cut with probability density function, gradient power (γ) and weighted factor of edge (ε) in graph cut based active contour are optimized at 0.5, 18 and 1, respectively.

3D Proposed segmentation result					
	%TPR ± SD	%DSC ± SD	%JSC ± SD	%VD ± SD	%FNR ± SD
Easy cases	96.50 ± 2.01	93.62 ± 1.55	88.04 ± 2.69	6.16 ± 4.26	3.50 ± 2.01
Difficult cases	96.01 ± 2.08	90.13 ± 2.94	82.15 ± 4.84	12.33 ± 6.89	2.91 ± 2.08
Mean	96.30 ± 2.00	91.88 ± 2.90	85.10 ± 4.86	9.25 ± 6.41	2.70 ± 2.00

Table 2
Optimization of the proposed method by modifying the weighted factor variance (α) in graph cut with probability density function, contour neighborhood voxel size (β), gradient power (γ) and weighted factor of edge (ε) in graph cut based active contour. The reference parameter is $\alpha = 0.5$, $\beta = 9$, $\gamma = 18$ and $\varepsilon = 1$. The final optimized parameter is $\alpha = 0.5$, $\beta = 7$, $\gamma = 18$ and $\varepsilon = 0.2$.

Segmentation accuracy (%DSC)									
	reference	α		β		γ		ε		final optimized
		0.25	1	7	11	6	24	0.5	0.2	
Easy cases	93.33%	81.67%	83.96%	93.62%	92.80%	87.14%	86.44%	93.41%	92.67%	93.46%
Difficult cases	89.55%	84.01%	85.04%	89.86%	90.13%	82.31%	87.54%	88.37%	88.91%	89.45%
Mean	91.44%	82.84%	84.05%	91.88%	91.47%	84.73%	86.99%	90.89%	90.79%	91.46%

edge. For voxel width optimization, the β parameter is varied at 7, 9 and 11 voxels. For power magnitude of gradient optimization, the γ parameter is varied at 6, 18 and 24. For anisotrophic weighted edge optimization, the ε parameter is varied at 0.2, 0.5 and 1. The result shows the improvement in the easy cases when using 7 as compared with using 11. In contrast, in the difficult cases, using 11 as the voxel width is better than using 7. However, the overall accuracy of using 7 is slightly better than using 11 as the voxel size, as shown in Table 2 and Fig. 7. The gradient strength in GCBAC is also important factor. The power magnitude at 6 is too weak and 24 is too strong for 3D AAA segmentation, which could lower the segmentation accuracy as compared with the power magnitude of 18, as shown in Table 2. Furthermore, at the region of aortic slope such as aortic bifurcation, the contour is not fitting enough to the slope, so the other optimization is required. The other optimization of the proposed method relies on the anisotropic weighted edge or assigning the weighted edges using different weights. For the anisotropic weighted edge ($\varepsilon = 0.2$ and 0.5), the overall accuracy is not significant different from the isotropic weighted

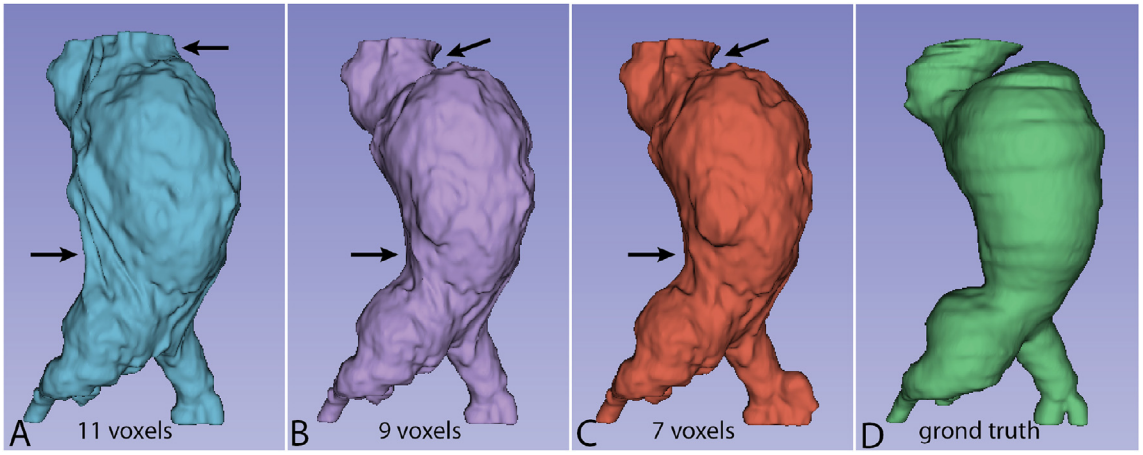

Fig. 7. Optimization of voxel size of contour neighborhood in the graph cut based active contour. (A)–(C) are optimization of voxel size of 11, 9, 7 respectively. Smaller voxel size is more fit to the contour of the outer wall (arrow). (D) is the ground truth segmentation.

Table 3
Selected cases with benefit on using anisotropic weight edge in the graph cut based active contour. There are 6 cases (2 easy and 4 difficult cases) from 20 cases, which have benefit of using anisotropic weighted edge on the graph cut based active contour. Only 2 (*) from 6 cases shows the significant improvement of the segmentation result, when using anisotropic weighted edge ($\varepsilon = 0.2$). The weighted factor variance (α) in graph cut with probability density function and gradient power (γ) in graph cut based active contour are optimized at 0.5 and 18, respectively.

Segmentation accuracy (%DSC ± SD)				
	11 voxels	9 voxels	7 voxels	7 voxels + anisotropic weighted edge
case 1 (easy)	94.11%	93.62%	94.00%	94.32%
case 2 (easy)	89.28%	89.32%	89.77%	89.92%
case 3 (difficult)	88.05%	88.88%	89.59%	89.66%
case 4 (difficult)	89.10%	89.33%	88.69%	92.57%*
case 5 (difficult)	90.93%	90.90%	90.98%	91.10%
case 6 (difficult)	94.15%	88.66%	89.15%	94.92%*

edge. However, the anisotropic weighted edge has benefit on some cases, in which the resulting contour is directly in the oblique direction from the aorta just above the bifurcation to iliac artery as shown in Tables 2 and 3 and Fig. 8. In these cases, the anisotropic weighted edge significantly improves the segmentation result. For example, the case No.6 in Table 3, the segmentation result (DSC value) improves from 89.15% to 94.92% by using the anisotropic weighted edge with the CN voxel size = 7.

The proposed segmentation algorithm successfully segmented all cases in the dataset. When compared with the gold standard, for the easy cases the proposed segmentation method achieved average TPR, DSC, JSC, VD and FNR values of 96.50 ± 2.01%, 93.62 ± 1.55%, 88.04 ± 2.69%, 6.16 ± 4.26% and 3.50 ± 2.01%, respectively. For the difficult cases, the proposed method achieved average TPR, DSC, JSC, VD and FNR values of 66.01 ± 2.08%, 90.13 ± 2.94%, 82.15 ± 4.84%, 12.33 ± 6.89% and 3.91 ± 2.08%, respectively, as shown in Fig. 6.

In the comparison between 2D and 3D versions of the proposed method, the 3D version is shown to have higher accuracy in average (91.88% versus 87.57%), as shown in Table 4. In addition, several stepping curves of the resulting contour were found in the 2D version. The 3D version produces smooth contours because there is only one graph for the entire object, whereas the 2D version performs the segmentation for each slice separately, as shown in Fig. 9.

The proposed 3D segmentation technique also outperforms the other existing 2D techniques on this dataset, as shown in Table 4 and Fig. 9. Our 3D technique generally results in a smoother segmented contour and more accurate segmentation at branches (iliac arteries). The 2D segmentation techniques also do not perform well in regions of curvature (slope) of the aorta, which is usually found in the case of

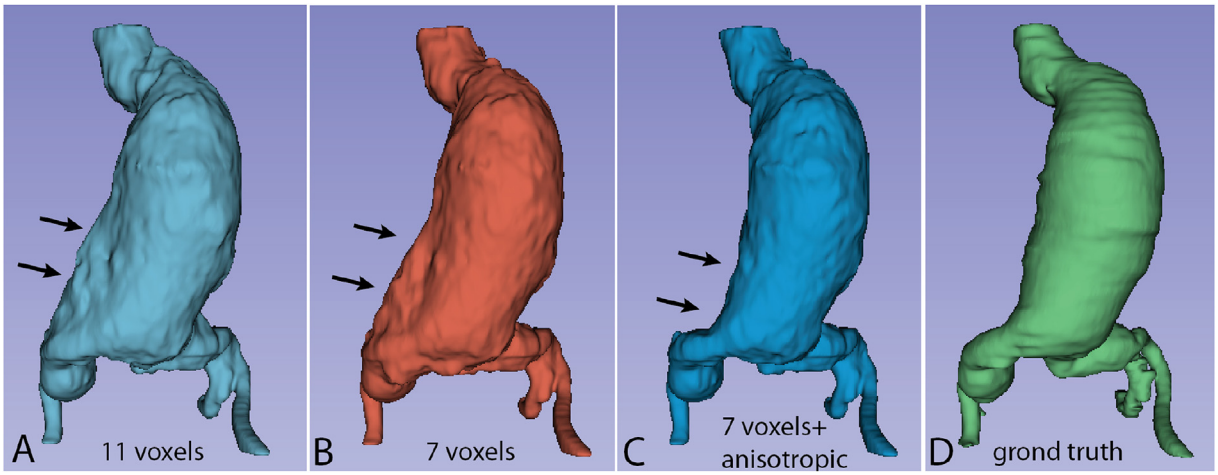

Fig. 8. Optimization of anisotropic weighted edge in the graph cut based active contour (GCBAC). From (A) to (B), using the smaller voxel size slightly increases the accuracy and fitting of the contour to the outer wall (arrow). (C) is anisotropic weighted edge in GCBAC showing significant improvement of the result, as compared with the ground truth segmentation (D).

Table 4
Quantitative comparison of the segmentation accuracy between the proposed method and previous studies. The easy and difficult cases were performed with the contour neighborhood voxel size = 7 and 11, respectively. The weighted factor variance (α) in graph cut with probability density function, gradient power (γ) and weighted factor of edge (ε) in graph cut based active contour are optimized at 0.5, 18 and 1, respectively.

Segmentation accuracy (%DSC ± SD)					
	3D proposed method	2D proposed method	2D GC	2D DRLSE	2D RGAC
Easy cases	93.6 ± 1.6%	89.9 ± 5.0%	71.8 ± 8.3%	55.2 ± 10.0%	82.0 ± 8.4%
Difficult cases	90.1 ± 2.9%	85.3 ± 2.5%	73.1 ± 8.3%	61.8 ± 5.9%	70.4 ± 9.3%
Mean	91.9 ± 2.9%	87.6 ± 4.5%	72.5 ± 8.1%	58.5 ± 8.9%	76.2 ± 10.5%

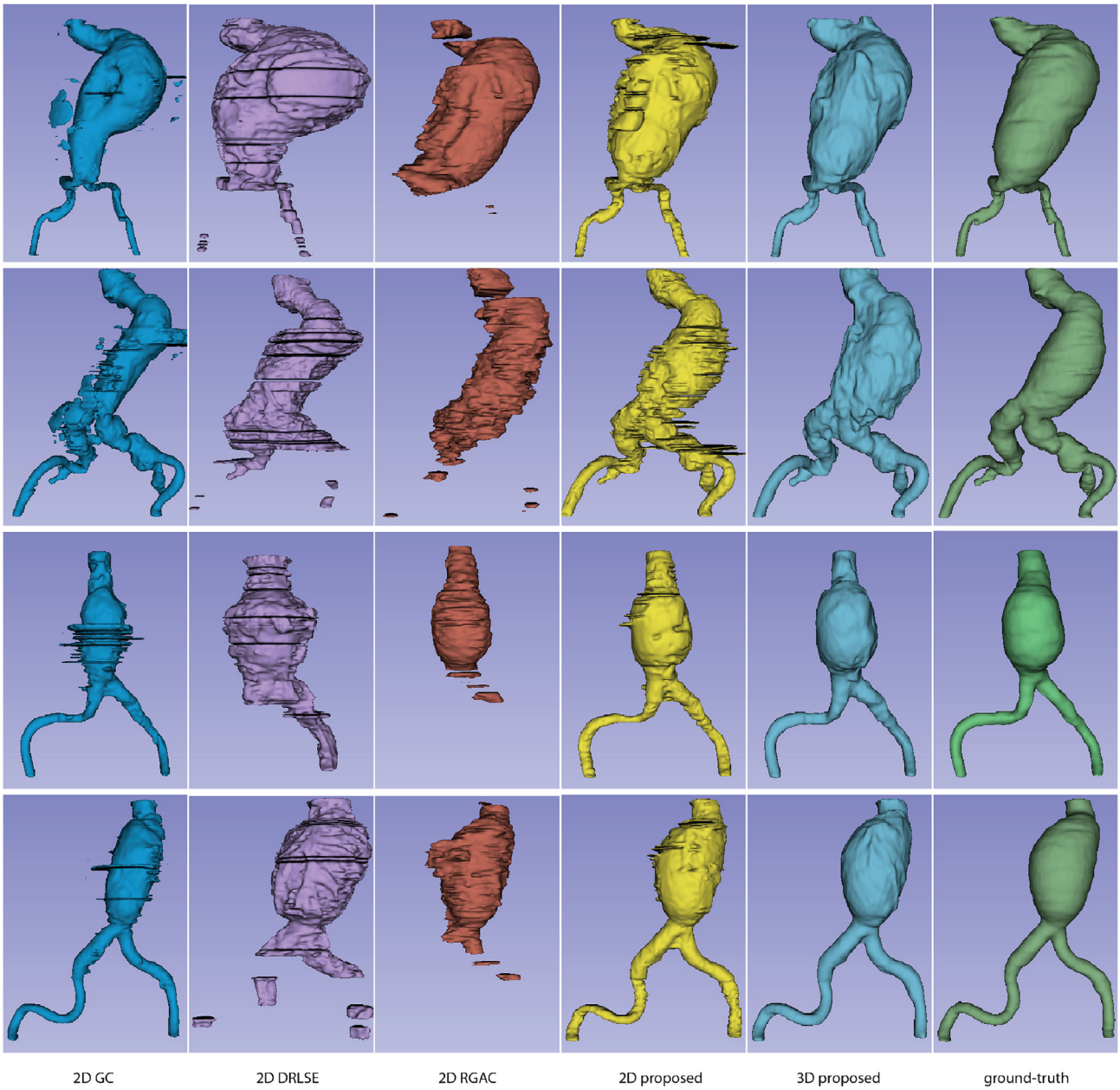

Fig. 9. Comparison of several segmentation methods on the same dataset. From the left to right columns, they are the segmentation results from the 2D graph-cut (GC), 2D distance regularized level set evaluation (DRLSE), 2D registered geographic active contour (RGAC), 2D version of the proposed method, 3D version of proposed methods and ground-truth, respectively. Two upper rows are two difficult cases and two lower rows are two easy cases. 2D DRLSE and 2D RGAC have the limitation at arterial branches. Our proposed method can solve the problem at arterial branches. 3D version of our proposed method has better segmentation result, when compared with the 2D version, which shows benefit on difficult cases more than easy cases. The segmentation accuracy of 2D and 3D version of our proposed methods are not significant different. However, on the visualization of 3D surface model, the 3D result is significant better.

aneurysm as described in the following paragraph.

The result (DSC value) of 2D-GC method on AAA segmentation is only 72.47%. The 2D-DRLSE and 2D-RGAC are the recent advanced segmentation methods which attain segmentation DSC accuracy of 58.5% and 76.21%, respectively. In addition, the 2D-RGAC gets the initial contour from the result of previous slices. Thus, when the 2D-RGAC fails to perform the segmentation, it cannot provide the initialization for the subsequent slices. In this case, the re-initialization on the failed slice is used to solve the problem. Differently, the 2D-DRLSE method separately segmented each image/slice by its own initial contour, so the re-initialization is not required.

4. Discussion

This paper has proposed the 3D segmentation of AAA using the concept of VNS [7–9] by iteratively alternating between two different segmentation techniques in the two different 3D search spaces of voxel intensity and voxel gradient. The proposed method has the potential to generally apply for difficult grayscale segmentation problems such as AAA, tumor and other organ segmentation. The segmentation provides accurate information for pre-operative planning of endovascular stent grating, volumetric follow up and predicting risk of rupture of AAA. The segmentation output of each method is used as the initial contour to the other method in each iteration. By alternating between search spaces, the technique can escape local minima that naturally occur in each search space. The first layer segmentation is based on the GCPDF, constructed using the 3D graph. The second layer segmentation relies on the contour-based technique, called GCBAC, which detects the boundary of an object depending on the gradient difference of the adjacent voxels [29].

Empirical analysis shows that when GCPDF and GCBAC are used alone for AAA segmentation they become trapped in somewhere in the background, which leads to poor accuracy. When one algorithm gets trapped in a local minimum, the other can help to escape it and enable the first algorithm to progress toward the optimal solution, as illustrated in Fig. 10. The figure shows that GCPDF is used as the initial segmentation technique. It starts to converge and then gets stuck in a local minimum at the 6th, 7th and 8th iterations. Then GCBAC is used after the 8th iteration to alter the move beyond that point in the search space. As a result, GCPDF escapes the local minimum and continues to make progress. This also happens at the 16th and 24th iterations. Our evaluation shows that the iterative combination of the two segmentations enables the segmentation result of the outer wall of AAA with high accuracy in both easy and difficult cases. The DSC value is 93.62 ± 1.55% and 90.13 ± 2.94% in easy and difficult cases, respectively (Table 1).

This proposed method has 2D and 3D versions. Because the proposed method is based on graph structures, the 2D version segments one case using several graphs, with one 2D graph used for each CT slice. The 3D version segments the whole volume of each case using only one 3D graph. The experimental results in the same dataset show that the overall accuracy of the segmentation of the 3D version is better than the 2D version, with the DSC value of 91.88% and 87.57%, respectively (Table 4). The detailed results show that the proposed method can solve the problem in the easy and difficult cases with good accuracy, as shown in Table 1. The difficult case has severe tortuosity of AAA visualized in bizarre shaped of aneurysm on 2D CT slice, as shown in Fig. 1. This cannot be solved using the 2D segmentation. The 3D segmentation is the solution to solve this problem. Even though, the 3D version has a little improvement of accuracy as compared with the 2D version about 3–4%, but the segmented contour is much smoother as shown in Fig. 7. The smooth and accurate segmented contour is an important key for the pre-operative planning and wall stress measurement. For this reason, the 3D version has significant benefit on the AAA segmentation. Furthermore, the proposed method is the first implementation of real 3D segmentation of AAA. The GCPDF and GCBAC techniques are based on graph structures, which can be easily generalized to N dimensions. The previous studies are difficult to solve the problem in N-Dimension of segmentation [11–13].

The GC is the intensity-based segmentation and commonly used in 2D and 3D medical images. Two recent advanced segmentation methods (DRLSE and RGAC) also performed on the same dataset to evaluate the accuracy. Both DRLSE and RGAC are the contour-based 2D segmentations, based on level set and geodesic active contours. The

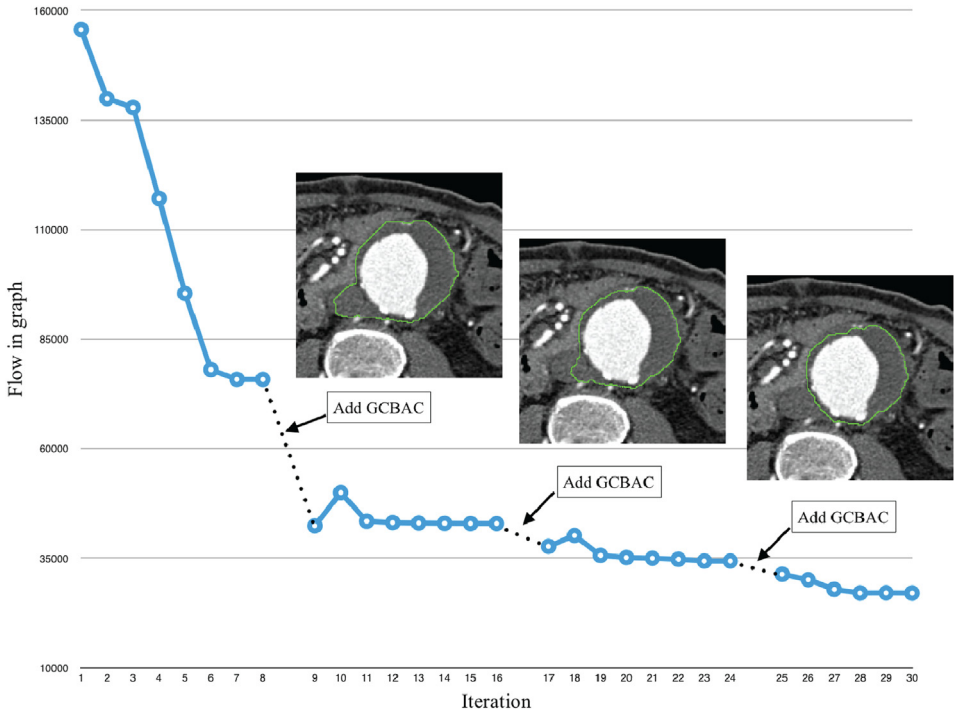

Fig. 10. Demonstration of concept of variable neighborhood search on outer wall segmentation. The chart of max-flow in graph in each iteration of graph cut with probability density function on AAA.

performance comparison shows that the segmentation accuracy of the 2D version of this proposed method, GC, DRLSE and RGAC are 87.55%, 72.47%, 58.50% and 76.21%, respectively (Table 4). The performance on the easy case is better than the performance on the difficult cases, except using the GC and DRLSE methods. The accuracy of GC is better than DRLSE, but most of slices at the region of aneurysm are reached at the inner lumen and worse than DRLSE to detect outer wall (Fig. 9). By the observation, the GC based method provides the good outer wall detection when the initial contour is proximity to the outer wall. The RGAC resulted in many failures on the contour detection because RGAC is to detect the outer wall in subsequent slices by relying on the segmentation result from the previous slice. An average of failure of contour detection of RGAC method is about 10 images per case. This required the re-initialization with the manual delineation, which is not practical in the routine use. The accuracy of DRLSE method is 58.50%. This is quite similar to previous study of Wang et al. [38] which reported the accuracy of DRLSE on their datasets with a DSC value of 55.56%. This proposed method can solve the problem of iliac branches segmentation, which cannot be solved by DRLSE and RGAC.

Parameter optimizations of this proposed method are also performed. The weighted factor or width of variance (α) in GCPDF is performed at 0.25, 0.5 and 1. The optimum value is 0.5. The value 0.25 is too narrow for the variation of pixel intensity of the thrombus, whereas the value 1 is too wide that includes other structures with much different pixel intensity into the result. The three parameters in GCBAC method are voxel width in CN (β), power magnitude of gradient (γ) and anisotropic weighted edge(ε). For voxel width optimization, the result shows some improvement of overall accuracy of the outer wall contour with 7 voxel width as shown in Fig. 7. Notice that result contour is more fit to the outer wall when it uses smaller voxel width, as shown in Fig. 9. The power magnitude of gradient is optimum at 18. The power magnitude at 6 is too weak, where the segmentation is usually shrink to inner wall. Whereas the power magnitude of 24 is too strong, where the segmentation is usually trapped at other structures. The anisotropic weighted edge is used to optimize in the case of result contour do not fit the slope of aortic bifurcation. Based on the prior knowledge of tubular shaped aorta, the outer wall of AAA should be also tubular in shaped. Applied this concept to the 3D graph cut segmentation, the edge connecting between each node in the graph in the vertical direction should be set up to be higher weighting factor, when compared with the orthogonal direction. The improvement is occurred at aortic bifurcation, as shown in Table 4 and Fig. 9. There are only two cases having great slope at aortic bifurcation, which cannot be solved by narrowing the voxel width in GCBAC. The other 18 cases do not have this problem. This is why the anisotropic weighted edge do not furthermore improve the accuracy.

Table 5 shows the comparisons with the previous methods [13–16,38]. All of them are based on the single segmentation with proper preprocessing step. Previous studies performed the 2D segmentation for each slice of contiguous CT images or 3D segmentation with manual interaction. de Bruijne et al. [13] proposed the segmentation method using the active shaped model in 3D with some manual interaction at the top and bottom contours. Lee et al. [14] proposed the inner and outer wall segmentations using graph on triangular mesh. The graph is constructed in 2D on the 3D surface of the triangular mesh to solve the 3D dataset problem. Several manual control points are still required for the segmentation. They reported the successful segmentation in four cases from the total of nine patient cases.

Olabarriaga et al. [15] proposed the segmentation approach using a 3D discrete deformable model with some manual interaction. Two manual interactions are defined in proximal and distal slices of the lumen for the initialization. They reported accuracy of segmentation in the range of 82.8%–96.8%. In this technique, the statistical gray level model depends on quality of training data with ground-truth (manual drawing), which is used for training the classifier. If the quality is poor, the result could be fail. Furthermore, since the deformable model is

Table 5
Performance summary of the proposed method and the previous studies on the detection of outer wall of abdominal aortic aneurysm. The methods are tested on different datasets. More details are provided in the discussion section.

Method	Datasets	2D/3D	Number of test cases	Accuracy (%DSC)	%error
Active shape model with intervene manual contour [13]	CT	3D	23	95.8%	3.5%–3.9%
Discrete deformable model with manual interaction [15]	CT	3D	17	95.0% (82.8%–96.8%)	0.4%–24.1%
Level set with morphological based initial contour [16]	CT	2D/3D	20	95.3% (92.9%–97.5%)	0.04%–7%
Graph search-based with manual control point [14]	CT	2D on 3D mesh	9	No DSC reported (success in 4 cases from the total of 9 cases)	–
Registration based geodesic active contour [38]	MR	2D	19	89.79% (85.35%–93.24%)	2.46%
Our proposed method (GCPDF + GCBAC)	CT	3D	20	91.88% (80.03%–95.45%)	2.90%

initialized from the inner lumen, if the thrombus is large, the segmentation result may fall inside the thrombus. In contrast, our proposed method initializes the outer wall from the dilation of inner lumen to cover the entire outer wall, which can solve the large size thrombus problem. The most effective recent method of AAA segmentation [16,38] is based on the active contour such as geodesic active contour or level set. Zhuge et al. [16] proposed outer wall segmentation in CTA by incorporating a possible region map following with the 3D level set. Since the possible region map uses only one 2D slice at a time, the method is not fully 3D. If the impossible region overlaps with the aneurysm, it results in missed detection. Nevertheless, they reported high accuracy of segmentation (95.3%). Lpez-Linares et al. [17] proposed machine learning based segmentation on post-operative AAA using CNN and holistically-nested edge detection. Their proposed method has the advantage of being a non-parametric approach. However, a large amount of specific training data is needed. With a dice score of about 82%, the accuracy of their segmentation algorithm is not better than that of previous studies. As compared with previous studies for volume difference, Freiman et al. [39], Zohios et al. [40] and Lpez-Linares et al. [17] report volume difference of 8%, 4%, and 11.6%, respectively. Our method produces comparable value of volume different of 9.25%. The CNN method [17] has the limitation of extending aneurysm to iliac artery, since the training data was not sufficient for that area. Our proposed method works well even though aneurysm occurs at the iliac artery. Our proposed method is considered as fully 3D parametric segmentation, based on the 3D graph constructed from the 3D dataset and does not require any manual interaction. The large size of thrombus inside AAA can be solved by our method. The method can also solve the case of the contiguous iliac branches from aorta, which have not been mentioned in any previous studies.

A limitation of our proposed method is that it requires an initial contour that must cover the outer wall. This algorithm is based on the graph structure to find the minimum cost inside area of search space. If the initial contour does not cover the outer wall, the resulted contour trends to shrink to inner wall. Calcifications may be present on the wall surface or embedded in the wall of AAA. We did not address calcifications on the proposed method. Based on the gradient property and minimum cut on graph-cut in our proposed method, the calcifications are usually outside of the segmentation result. However, the calcifications in AAA are usually small, and appeared as a thin layer. The number of calcifications is small and did not affect the overall accuracy of the segmentation.

5. Conclusion

This paper introduced a fully automated process for 3D segmentation of the outer wall of AAA, using the VNS concept that iteratively combines two different segmentation techniques. One technique searches through the intensity space and the another technique searches through the gradient space. This novel concept of segmentation has the potential to solve the difficult grayscale segmentation in the medical images. Furthermore, the 3D segmentation shows the better contour of the segmentation results, when compared with the 2D segmentation. The 3D segmentation also shows the advantage of branching vessel (iliac arterial branches) over the 2D segmentation. This novel proposed method successfully solves the difficult cases of AAA segmentation. It is the highly promising tool to reduce the time and effort to evaluate AAA in practice.

Acknowledgment

This work was partially supported through a grant from the Hanse-Wissenschaftskolleg Institute for Advanced Study, Delmenhorst, Germany to Haddawy for collaborative work with the University of Bremen.

References

[1] D. Sidloff, E. Choke, P. Stather, M. Bown, J. Thompson, R. Sayers, Mortality from thoracic aortic diseases and associations with cardiovascular risk factors, Circulation 130 (25) (2014) 2287–2294, https://doi.org/10.1161/CIRCULATIONAHA.114.010890.

[2] D. Sidloff, P. Stather, N. Dattani, M. Bown, J. Thompson, R. Sayers, E. Choke, Aneurysm global epidemiology study: public health measures can further reduce abdominal aortic aneurysm mortality, Circulation 129 (7) (2014) 747–753, https://doi.org/10.1161/CIRCULATIONAHA.113.005457.

[3] J. Upchurch, G. R, T.A. Schaub, Abdominal aortic aneurysm, Am. Fam. Physician 73 (7) (2006) 1198–1204.

[4] D.E. Lilienfeld, P.D. Gunderson, J.M. Sprafka, C. Vargas, Epidemiology of aortic aneurysms: I. mortality trends in the United States, 1951 to 1981, Arteriosclerosis 7 (6) (1987) 637–643.

[5] D.A. Vorp, Biomechanics of abdominal aortic aneurysm, J. Biomech. 40 (9) (2007) 1887–1902, https://doi.org/10.1016/j.jbiomech.2006.09.003.

[6] T. Siriapisith, W. Kusakunniran, P. Haddawy, Outer wall segmentation of abdominal aortic aneurysm by variable neighborhood search through intensity and gradient spaces, J Digit Imaging.doi:10.1007/s10278-018-0049-z.

[7] P. Hansen, N. Mladenovi, Developments of Variable Neighborhood Search, Springer US, Boston, MA, 2002, pp. 415–439, https://doi.org/10.1007/978-1-4615-1507-4_19.

[8] P. Hansen, N. Mladenovi, J.A. Moreno Prez, Variable neighbourhood search: methods and applications, Ann. Oper. Res. 175 (1) (2010) 367–407, https://doi.org/10.1007/s10479-009-0657-6.

[9] N. Mladenovi, P. Hansen, Variable neighborhood search, Comput. Oper. Res. 24 (11) (1997) 1097–1100 https://doi.org/10.1016/S0305-0548(97)00031-2.

[10] J. Shum, E.S. DiMartino, A. Goldhamme, D.H. Goldman, L.C. Acker, G. Patel, J.H. Ng, G. Martufi, E.A. Finol, Semiautomatic vessel wall detection and quantification of wall thickness in computed tomography images of human abdominal aortic aneurysms, Med. Phys. 37 (2) (2010) 638–648, https://doi.org/10.1118/1.3284976.

[11] E.K. Shang, E. Lai, A.M. Pouch, R. Hinmon, R.C. Gorman, r. Gorman, J. H, C.M. Sehgal, G. Ferrari, J.E. Bavaria, B.M. Jackson, Validation of semiautomated and locally resolved aortic wall thickness measurements from computed tomography, J. Vasc. Surg. 61 (4) (2015) 1034–1040, https://doi.org/10.1016/j.jvs.2013.11.065.

[12] E.K. Shang, D.P. Nathan, E.Y. Woo, R.M. Fairman, G.J. Wang, R.C. Gorman, r. Gorman, J. H, B.M. Jackson, Local wall thickness in finite element models improves prediction of abdominal aortic aneurysm growth, J. Vasc. Surg. 61 (1) (2015) 217–223, https://doi.org/10.1016/j.jvs.2013.08.032.

[13] M. de Bruijne, B. van Ginneken, M.A. Viergever, W.J. Niessen, Interactive segmentation of abdominal aortic aneurysms in cta images, Med. Image Anal. 8 (2) (2004) 127–138 https://doi.org/10.1016/j.media.2004.01.001.

[14] K. Lee, Y. Johnson Rk Fau Yin, A. Yin Y Fau Wahle, M. E. Wahle A Fau Olszewski, T. D. Olszewski Me Fau Scholz, M. Scholz Td Fau Sonka, M. Sonka, Three-dimensional Thrombus Segmentation in Abdominal Aortic Aneurysms Using Graph Search Based on a Triangular Mesh (1879-0534 (Electronic)).

[15] S. D. Olabarriaga, M. Rouet Jm Fau Fradkin, M. Fradkin M Fau Breeuwer, W. J. Breeuwer M Fau Niessen, W. J. Niessen, Segmentation of Thrombus in Abdominal Aortic Aneurysms from Cta with Nonparametric Statistical Grey Level Appearance Modeling (0278-0062 (Print)).

[16] F. Zhuge, S. Rubin Gd Fau Sun, S. Sun S Fau Napel, S. Napel, An Abdominal Aortic Aneurysm Segmentation Method: Level Set with Region and Statistical Information (0094-2405 (Print)).

[17] K. Lpez-Linares, N. Aranjuelo, L. Kabongo, G. Maclair, N. Lete, M. Ceresa, A. Garca-Familiar, I. Maca, M.A. Gonzlez Ballester, Fully automatic detection and segmentation of abdominal aortic thrombus in post-operative cta images using deep convolutional neural networks, Med. Image Anal. 46 (2018) 202–214, https://doi.org/10.1016/j.media.2018.03.010.

[18] H. He, B. Upcroft, Grabcutsfm: How 3d Information Improves Unsupervised Object Segmentation, pp. 548–553. doi:10.1109/AIM.2013.6584149.

[19] W. Liao, Z. Tu, S. Wang, Y. Li, R. Zhong, H. Zhong, Compressed-domain video synopsis via 3d graph cut and blank frame deletion, Thematic Workshops 2017 - Proceedings of the Thematic Workshops of ACM Multimedia 2017, co-located with MM, 2017, pp. 253–261, , https://doi.org/10.1145/3126686.3126778.

[20] D. Grosgeorge, C. Petitjean, B. Dubray, S. Ruan, Esophagus segmentation from 3d ct data using skeleton prior-based graph cut, Comput. Math. Methods Med. 2013 (2013) 6, https://doi.org/10.1155/2013/547897.

[21] M. Eapen, R. Korah, G. Geetha, Swarm intelligence integrated graph-cut for liver segmentation from 3d-ct volumes, Sci. World J. 2015 (2015) 12, https://doi.org/10.1155/2015/823541.

[22] L. Massoptier, S. Casciaro, Fully automatic liver segmentation through graph-cut technique, 29th Annual International Conference of the IEEE Engineering in Medicine and Biology Society, 2007, pp. 5243–5246, , https://doi.org/10.1109/IEMBS.2007.4353524.

[23] J. Cha, M.M. Farhangi, N. Dunlap, A.A. Amini, Segmentation and tracking of lung nodules via graph-cuts incorporating shape prior and motion from 4d ct, Med. Phys. 45 (1) (2018) 297–306, https://doi.org/10.1002/mp.12690.

[24] J. w. Cha, N. Dunlap, B. Wang, A. Amini, 3d segmentation of lung ct data with graph-cuts: analysis of parameter sensitivities, in: SPIE Medical Imaging, Vol. vol. 9788, SPIE, p. 7.

[25] U. Yoruk, B.A. Hargreaves, S.S. Vasanawala, Automatic renal segmentation for mr urography using 3d-grabcut and random forests, Magn. Reson. Med. 79 (3) (2018)

1696–1707, https://doi.org/10.1002/mrm.26806.
[26] C. Rother, V. Kolmogorov, A. Blake, "grabcut" - interactive foreground extraction using iterated graph cuts, in: ACM Trans. Graph., Vol. 23, pp. 309–314. doi:10.1145/1015706.1015720.
[27] K. Li, X. Wu, D.Z. Chen, M. Sonka, Optimal surface segmentation in volumetric images-a graph-theoretic approach, IEEE Trans. Pattern Anal. Mach. Intell. 28 (1) (2006) 119–134, https://doi.org/10.1109/tpami.2006.19.
[28] X. Chen, J.K. Udupa, U. Bagci, Y. Zhuge, J. Yao, Medical image segmentation by combining graph cuts and oriented active appearance models, IEEE Trans. Image Process. A Publ. IEEE Signal Process. Soc. 21 (4) (2012) 2035–2046, https://doi.org/10.1109/TIP.2012.2186306.
[29] N. Xu, N. Ahuja, R. Bansal, Object segmentation using graph cuts based active contours, Comput. Vis. Image Understand. 107 (3) (2007) 210–224 https://doi.org/10.1016/j.cviu.2006.11.004.
[30] T.J. Atherton, D.J. Kerbyson, Size invariant circle detection, Image Vis Comput. 17 (1) (1999) 795–803.
[31] W. He, L. Zhang, H. Yang, Z. Jiang, H. Zhang, W. Shi, Y. Miao, F. He, A study of multilevel banded graph cuts for three-dimensional colon tissue segmentation, Int. J. Pattern Recogn. Artif. Intell. 31 (9). doi:10.1142/S0218001417550126.
[32] H. Shigeta, T. Mashita, J. Kikuta, S. Seno, H. Takemura, M. Ishii, H. Matsuda, Bone marrow cavity segmentation using graph-cuts with wavelet-based texture feature, J. Bioinf. Comput. Biol. 15 (5). doi:10.1142/S0219720017400042.
[33] Y.Z. Zeng, Y.Q. Zhao, P. Tang, M. Liao, Y.X. Liang, S.H. Liao, B.J. Zou, Liver vessel segmentation and identification based on oriented flux symmetry and graph cuts, Comput. Methods Progr. Biomed. 150 (2017) 31–39, https://doi.org/10.1016/j.cmpb.2017.07.002.
[34] V. Kolmogorov, R. Zabih, What Energy Functions Can Be Minimized via Graph Cuts? (0162-8828 (Print)).
[35] D.R. Ford, D.R. Fulkerson, Flows in Networks, Princeton University Press, 2010.
[36] L. Chunming, X. Chenyang, G. Changfeng, D.F. Martin, Distance regularized level set evolution and its application to image segmentation, IEEE Trans. Image Process. 19 (12) (2010) 3243–3254, https://doi.org/10.1109/TIP.2010.2069690.
[37] Y. Chen, L. Navarro, Y. Wang, G. Courbebaisse, Segmentation of the thrombus of giant intracranial aneurysms from ct angiography scans with lattice Boltzmann method, Med. Image Anal. 18 (1) (2014) 1–8, https://doi.org/10.1016/j.media.2013.08.003.
[38] Y. Wang, F. Seguro, E. Kao, Y. Zhang, F. Faraji, C. Zhu, H. Haraldsson, M. Hope, D. Saloner, J. Liu, Segmentation of lumen and outer wall of abdominal aortic aneurysms from 3d black-blood mri with a registration based geodesic active contour model, Med. Image Anal. 40 (2017) 1–10 https://doi.org/10.1016/j.media.2017.05.005.
[39] M. Freiman, S.J. Esses, L. Joskowicz, J. Sosna, An iterative model-constrained graph-cut algorithm for abdominal aortic aneurysm thrombus segmentation, IEEE International Symposium on Biomedical Imaging: from Nano to Macro, 2010, pp. 672–675, , https://doi.org/10.1109/ISBI.2010.5490085.
[40] C. Zohios, G. Kossioris, Y. Papaharilaou, Geometrical methods for level set based abdominal aortic aneurysm thrombus and outer wall 2d image segmentation, Comput. Methods Progr. Biomed. 107 (2) (2012) 202–217 https://doi.org/10.1016/j.cmpb.2011.06.009.